Received: 12 July 2026 | Revised: 2 September 2026 | Accepted: 3 September 2026

DOI: 10.1111/jmi.70171

Journal of Microscopy RMS

RAPID PUBLICATION

Brillouin–Raman micro-mapping of silicone-hydrogel contact lenses: Revealing chemical and mechanical heterogeneities

Alessandra Anna Passeri[1] | **Martina Alunni Cardinali**[1,2] | **Erika Ponzini**[3,4] | **Silvia Tavazzi**[3,4] | **Daniele Fioretto**[1]

[1]Dipartimento di Fisica e Geologia, Università di Perugia, Perugia, Italy

[2]Dipartimento di Chimica, Biologia e Biotecnologie, Università di Perugia, Perugia, Italy

[3]Department of Materials Science, University of Milano-Bicocca, Milan, Italy

[4]COMiB Research Centre in Optics and Optometry, University of Milano-Bicocca, Milan, Italy

Correspondence
Daniele Fioretto, Dipartimento di Fisica e Geologia, Università di Perugia, Perugia, Italy.
Email: daniele.fioretto@unipg.it

Funding information
the CARIT Foundation

Abstract

Joint Brillouin–Raman micro-spectroscopy (BRMS) enables simultaneous, non-destructive characterisation of the mechanical and chemical properties of soft materials at the micrometre scale, combining GHz-range viscoelastic information from acoustic modes with the vibrational fingerprint of molecular species. We present an improved BRMS platform based on an inverted microscope with a single confocal pinhole shared by both spectrometers allowing a single spectrum spanning from 0.1 GHz to 100 THz to be acquired at each point of a raster scan. Applied to Delefilcon A silicone-hydrogel contact lenses, macroscopically homogeneous and optically transparent, the platform reveals micrometric bulk heterogeneities not previously reported. Their Raman fingerprint identifies these features as clusters of the copper phthalocyanine handling tint. Two-dimensional Brillouin mapping shows a reduction of the frequency shift by up to ~0.5 GHz near the cluster centres, corresponding to a decrease of about 12% in the longitudinal elastic modulus. These results demonstrate the ability of BRMS to resolve chemical–mechanical heterogeneities that are inaccessible to either technique alone, with potential implications for the durability of biomedical soft materials.

KEYWORDS

Brillouin microscopy, confocal spectroscopy, material heterogeneity, micro-mechanical mapping, Raman spectroscopy, silicone-hydrogel contact lenses

1 | INTRODUCTION

Brillouin spectroscopy probes the frequency shift and linewidth of light scattered by thermally activated acoustic modes, enabling the non-destructive viscoelastic characterisation of condensed matter in the GHz frequency regime[1,2] with micrometric spatial resolution.[3] These features have made it increasingly valuable across a broad range of scientific and technological applications.[4,5] Introduced roughly two decades ago, Brillouin microscopy and imaging have recently undergone rapid development,[6] particularly for ophthalmological applications,[7,8] largely driven by faster and more efficient optical spectrometers.

Recently, instruments capable of performing simultaneous Raman measurements have been developed;[9] Raman spectroscopy probes vibrational modes at frequencies

above the THz range, which can be related to the concentration of the different molecular species. Joint Brillouin–Raman micro-spectroscopy (BRMS) is attracting increasing attention for the correlative investigation of mechanical and chemical properties, particularly in complex systems such as biological materials or those intended for biomedical applications, where it is essential to relate properties and functions to the underlying mechanical and chemical structure at the microscopic scale.

In this work, we demonstrate the potential of an improved Brillouin–Raman spectrometer based on an inverted microscope and a confocal configuration shared by both spectrometers, an arrangement ideally suited to reaching the spatial resolution limits of BRMS thanks to the automatic matching of the scattering volumes. We employ BRMS to investigate the composition and mechanical properties of Delefilcon A contact lenses, which feature a silicone-hydrogel core with a relatively low water content (approximately 33%) covered by a thin (6–8 μm) layer of a highly hydrophilic hydrogel; this outer layer has a nominal equilibrium water content exceeding 80% and is intended to provide enhanced comfort during wear.[10,11] Previous Raman spectroscopy (RS) studies have corroborated both the nominal surface thickness and the presence of the water gradient at the lens interface.[12] In those investigations, the intensities of the CH_2 and CH_3 vibrational bands in the range 2800–3150 cm^{-1} characteristic of silicone hydrogel (SiHy) materials[13] were used to quantify the silica content within the polymer matrix. Here we demonstrate that the lenses exhibit several types of micrometric and sub-micrometric heterogeneities, both at the surface and within the bulk, which are characterised by the combined chemical–mechanical analysis. This type of study is clearly of interest for the further improvement of such lenses, particularly with regard to their degradation during use.

2 | MATERIALS AND METHODS

The measurements were performed on Delefilcon A contact lenses with an optical power of −0.50 dioptres. The lenses were kept fully submerged throughout the acquisitions in a preservative-free, buffered, isotonic, sterile saline solution (Isosol, VitaResearch, Rome, Italy). Delefilcon A lenses contain a handling tint—typically copper phthalocyanine—added at a very low concentration. Its sole purpose is to make the lens visible during handling (in the blister pack or soaking solution), since a fully transparent lens would be nearly invisible in liquid. The concentration is low enough that it does not affect vision or the wearer's perceived eye colour.

Micro-spectroscopic measurements were performed at the GHOST laboratory in Perugia, using an upgraded version of the setup described in in previous works.[9,14] The new apparatus (Figure 1) is based on an inverted microscope and features a single confocal pinhole shared by both spectrometers. Light from a single-mode green laser (Excelsior, Spectra-Physics, Milpitas, California, USA; λ = 532 nm) is delivered to the sample through a water-immersion objective (UPLSAPO 60XW, Olympus Tokyo, Japan; NA = 1.2), which also collects the back-scattered light. Laser power was lower than 15 mW to avoid sample damage. This light is focused by an achromatic lens onto a pinhole placed upstream of the spectrometers, realising the confocal configuration. Beyond the pinhole, an edge filter detuned by 1 THz from the laser line splits the signal: the quasi-elastic component is directed to the Brillouin spectrometer (TFP-2 HC, JRS Scientific Instruments, Mettmenstetten, Switzerland), while the higher-frequency-shifted component is sent to the Raman spectrometer (Triax, Jobin-Yvon, Palaiseau, France). This design allows Brillouin and Raman spectra to be acquired from the same point simultaneously. In this confocal configuration, the spatial resolution is approximately 0.5 μm laterally and 3–4 μm axially. The sample was mounted on top of a motorised Precision Linear Stage PLS85 (PI mi Cos), allowing the raster scans of the sample along x, y and z directions with sub-micrometric precision.

For each pixel of the maps, the spectroscopic signal was integrated for 2 min. This relatively long acquisition time was necessary to obtain a satisfactory signal-to-noise ratio in the Raman spectra, which are typically much weaker than the Brillouin signal and therefore set the lower bound on the dwell time per point.

Spectral analysis was performed using a custom Python script developed in-house. Brillouin spectra were fitted with a damped harmonic oscillator (DHO) lineshape,

$$I(\omega) = \frac{I_0}{\pi} \frac{\Gamma\Omega^2}{\left(\omega^2 - \Omega^2\right)^2 + \left(\Gamma\omega\right)^2}, \tag{1}$$

numerically convolved with the instrument response function $R(\omega)$ before comparison with the experimental data.[14] The three free fit parameters, Ω, Γ, and I_0, correspond to the Brillouin frequency shift, the full width at half maximum (FWHM) of the peak, and the integrated intensity of the Brillouin doublet, respectively. The values of Ω and Γ are related to the real and imaginary parts of the complex longitudinal modulus $M^*(\omega)$ evaluated at $\omega = \Omega$ by

$$M'(\Omega) = \frac{\rho_0}{q^2}\,\Omega^2, \tag{2}$$

$$M''(\Omega) = \frac{\rho_0}{q^2}\,\Gamma\Omega, \tag{3}$$

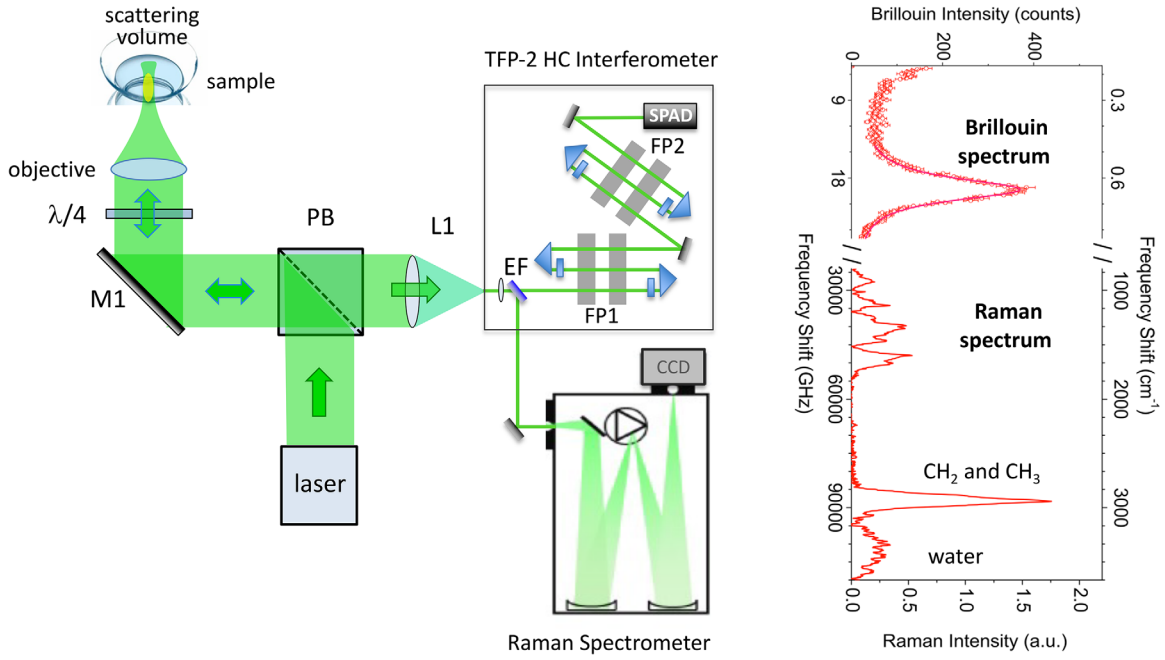

FIGURE 1 Schematic of the Brillouin–Raman micro-spectroscopy (BRMS) setup at the GHOST laboratory in Perugia. (Left) A single-mode green laser is delivered to the sample through a water-immersion objective, which also collects the back-scattered light. A quarter-wave plate ($\lambda/4$) and a polarising beamsplitter (PB) separate incident and scattered beams; the latter is focused by an achromatic lens (L1) onto a confocal pinhole placed upstream of both spectrometers. An edge filter (EF) then splits the signal: the quasi-elastic component is directed to a tandem Fabry–Pérot interferometer (TFP-2 HC), which uses two synchronously scanned Fabry–Pérot cavities (FP1, FP2) and a single-photon avalanche detector (SPAD); the higher-frequency-shifted component is sent to the Raman spectrometer (Triax, Jobin-Yvon), equipped with a CCD detector. (Right) Representative Brillouin and Raman spectra acquired simultaneously from the same point of a sample.

where ρ_0 is the mass density and q the wavevector in the medium. In the back scattering geometry here adopted $q = n\ 4\pi/\lambda_0$, n is the real part of the refractive index of the medium λ_0 is the wavelength in vacuum of the laser source. The same setup was also used for bright-field microscopy, as it is equipped with a white-light illuminator and a CCD camera that can be alternately inserted into the optical path to acquire images from the same sample region analysed by the raster-scan spectroscopic maps.

3 | RESULTS AND DISCUSSION

Although all examined lenses appear macroscopically homogeneous and optically transparent, bright-field microscopy combined with micro-spectroscopic analysis of local molecular composition and mechanical properties reveals heterogeneities, located both near the surface and within the bulk. Surface heterogeneities were analysed in a previous work,[15] consisting of micrometre regions with local reduction or absence of the surface layer of highly hydrophilic hydrogel. This effect is not visible via bright-field microscopy due to the almost absent contrast in refractive index between bulk water and highly hydrated hydrogel and was revealed via Brillouin-Raman maps. Conversely, micrometre size bulk heterogeneities are well visible also in bright-field images. To the best of our knowledge, the existence of these heterogeneities was never reported in previous works. In the following, we focus on the characterisation of these bulk heterogeneities, which are of interest as potential weak points affecting lens durability during use.[16]

3.1 | Bright-field microscopy

To distinguish systematic features from occasional manufacturing defects, bright-field images were acquired on lenses from six different production batches of Delefilcon A. Point-like inhomogeneities, localised within the silicone-hydrogel core, were consistently observed in all lenses examined. A typical image is reported in the inset of Figure 2. The optical contrast is quite high, which points to a sizeable difference in optical absorption with respect to the surrounding hydrogel matrix. Photos taken at different depths and on different samples show typical dimensions very close to the optical resolution of the setup. The chemical nature and the mechanical signature of these inhomogeneities are further investigated through BRMS measurements.

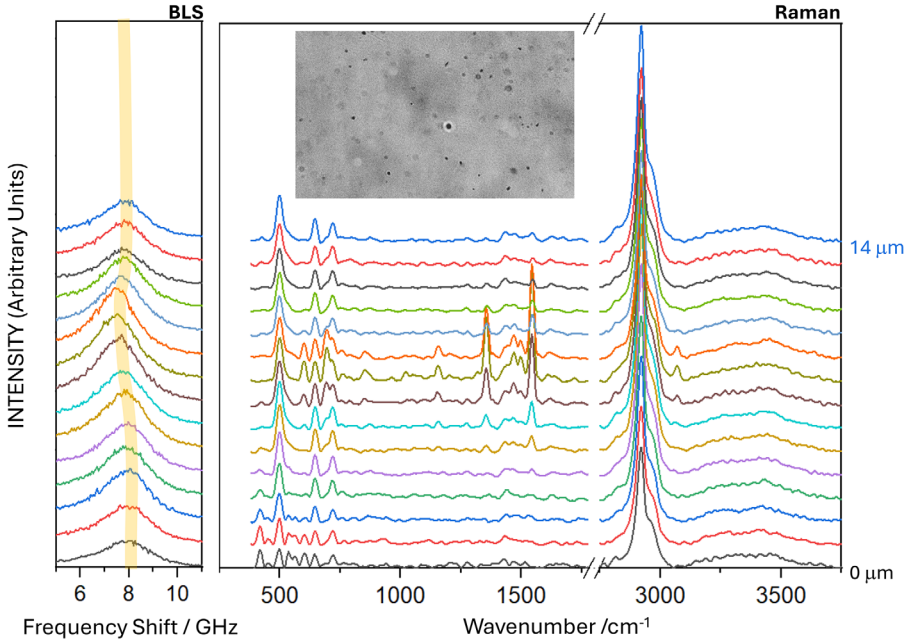

FIGURE 2 Brillouin (left) and Raman (right) spectra acquired along a linear depth scan on a Delefilcon A contact lens, from the surface (bottom) down to 14 µm inside the sample (top), with a step of 1 µm. The scan crosses one of the bulk inhomogeneities visible in the 100 × 60 µm bright-field image reported in the inset (top). The yellow shaded band in the left panel is a guide to the eye, highlighting the change in the Brillouin frequency shift with depth.

3.2 | BRMS in the silicone–hydrogel core

Figure 2 shows Brillouin and Raman spectra acquired on a lens along a linear scan as a function of the distance from the surface, down to a depth of 14 µm with 1 µm steps. The scan was performed so as to cross one of the inhomogeneity recorded in bright-field images of the sample (inset of Figure 2). In the Raman spectra, the CH-stretching region around 2900 cm^{-1} is clearly visible,[15] and its intensity grows progressively relative to that of the OH-stretching band around 3400 cm^{-1}, as expected for a decrease in water concentration and a corresponding increase in polymer-matrix concentration on moving towards the interior of the lens.[15] More interesting is the change in the Raman spectrum observed at a depth of about 8 µm, where features appear around 1400 cm^{-1} in coincidence with the crossing of the inhomogeneity. The simultaneous presence of spectral bands at approximately 590, 680, 1144, 1336, 1448, and 1522 cm^{-1} is consistent with the presence of copper phthalocyanine.[17] Indeed, according to Basova et al.,[18] the bands at 590 and 1336 cm^{-1} are attributed to vibrations of the macrocycle ring, while those at 680 and 1448 cm^{-1} correspond to stretching and bending modes of the isoindole groups. The band at 1144 cm^{-1} involves N_α–C_α–N_β, C_β–C_γ–H, and C_δ–C_δ modes, and the prominent signal at 1522 cm^{-1} originates from C_α–C_β, C_α–N_β, and C_β–C_β vibrations. In the range 500–700 cm^{-1}, there are also contributions due to the vibration of the siloxanes, whose intensity increases approaching the core of the lens.

Moreover, a substantial enhancement of the Raman scattering cross-section of these modes in our spectra was observed using red laser excitation relative to green light (data not shown), consistent with pre-resonance effects[19] that amplify the Raman signal of copper phthalocyanine using a green laser source.

Comparison of the Raman and Brillouin spectra acquired along the same linear scan reveals a marked reduction in both the frequency shift and the linewidth of the Brillouin peak, coincident with the appearance of the copper phthalocyanine Raman signal. Looking at Equations (1) and (2), this reduction may be associated with two possible scenarios: (i) a local softening of the lens, or (ii) a local reduction of the ratio n^2/ρ_0. Given the difficulty of measuring the refractive index within micrometric volumes inside a material, we attempt to discriminate between these two scenarios by means of a two-dimensional Brillouin mapping that encompasses several inhomogeneities of the lens.

Figure 3A shows a 14 × 22 μm^2 *xy* light micrograph of a region inside a contact lens, in which five distinct inclusions are visible, some closer to and some farther from the focal plane of the objective. A BRMS raster scan with a 1 µm step was performed over the same region. Equation (1) was fitted to the Brillouin spectrum acquired

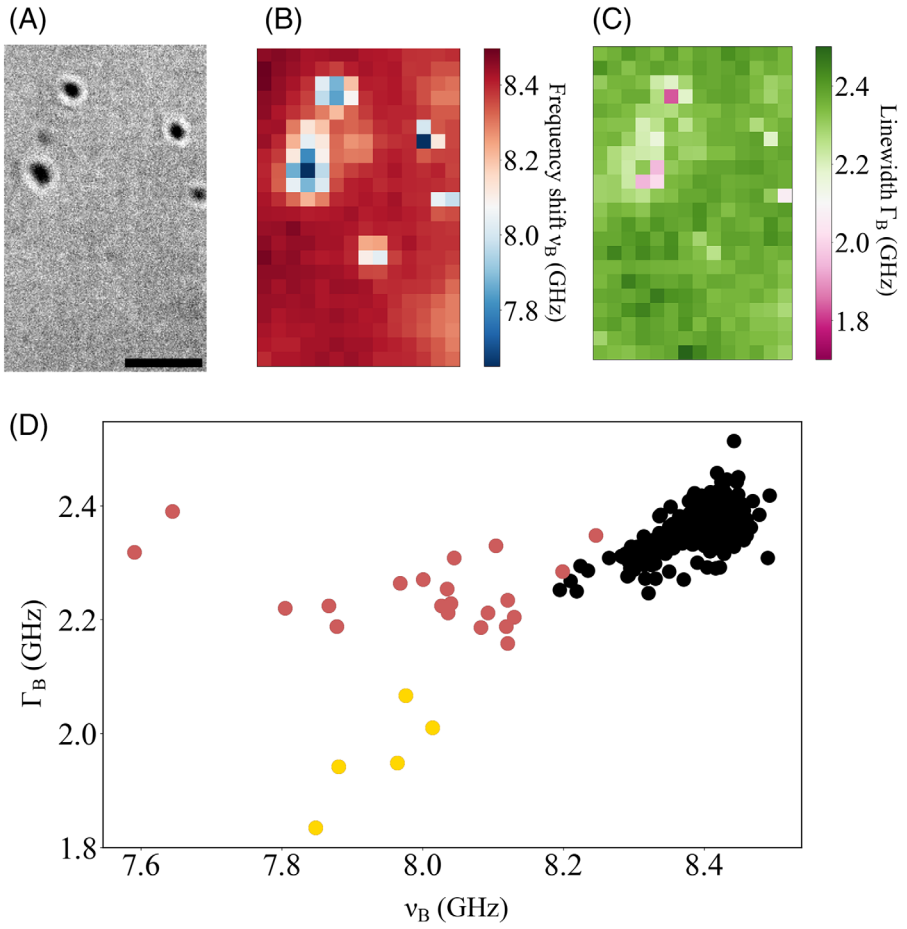

FIGURE 3 BRMS mapping of bulk inhomogeneities in a Delefilcon A contact lens. (A) Bright-field micrograph ($14 \times 22\ \mu m^2$) of a region inside the lens, showing five distinct inclusions at different distances from the focal plane of the objective; scale bar: 5 μm. (B, C) Two-dimensional maps of the Brillouin frequency shift $\nu_B = \Omega/2\pi$ and linewidth $\Gamma_B = \Gamma/2\pi$, obtained from a BRMS raster scan of the same region with a 1 μm step, by fitting Equation (1) to the Brillouin spectrum acquired at each point. (D) Brillouin linewidth Γ_B versus frequency shift ν_B for all points of the map: black circles correspond to points far from the inhomogeneities, yellow circles to points close to the centre of the inhomogeneities, and red circles to points at the boundary between the inhomogeneities and the surrounding lens matrix.

at each point, and the resulting values of the frequency shift $\nu_B = \Omega/2\pi$ and linewidth $\Gamma_B = \Gamma/2\pi$ are reported in Figure 3B and C, respectively. A clear correlation is apparent between the changes in the BLS maps (Figure 3B and C) and the presence of inhomogeneities in the bright-field image (Figure 3A). In particular, a reduction of the Brillouin frequency of up to ~0.5 GHz is observed close to the centre of the inclusions, corresponding to a decrease of approximately 12% in the elastic modulus, assuming that n^2/ρ_0 remains constant.

To better characterise the changes in the BLS parameters, Figure 3D shows the Brillouin linewidth versus the frequency shift for all points of the map. Black circles correspond to points far from the inhomogeneities, yellow circles to points close to the centre of the inhomogeneities, and red circles to points at the boundary between the inhomogeneities and the surrounding lens matrix. The black and yellow circles trace a coherent trend, consistent with the behaviour expected in soft matter with a mechanical relaxation lying at frequencies higher than those probed by BLS, which shifts in frequency in response to local changes in, for example, water concentration[20] or cross-link density. Although this behaviour does not entirely rule out a contribution from local variations of the refractive index, it suggests that a significant part of the observed reduction in the BLS parameters originates from a local softening of the lens.

This interpretation is further supported by a consistency check on the length scales involved. The coherence length of the probed acoustic modes—of the order of the acoustic wavelength Λ multiplied by the acoustic quality factor Ω/Γ obtained from the DHO fit[21]—is approximately 1.2 μm, whereas the typical size of the copper phthalocyanine inclusions is below 0.5 μm. A Brillouin line hypothetically generated by acoustic modes confined within one such inclusion would therefore exhibit a linewidth comparable

to its own frequency, in contrast with our observations. Taken together, these arguments support the first scenario, namely the existence of micrometric regions around the copper phthalocyanine inclusions that are softer than the surrounding lens.

Finally, the excess linewidth found in the spectra acquired at the boundary regions (red points in Figure 3) can be readily explained by heterogeneous broadening, that is, by the simultaneous scattering from phonons in the inhomogeneity and from phonons in the surrounding lens matrix, both intercepted within the scattering volume.

4 | CONCLUSIONS

We have shown that joint Brillouin–Raman microspectroscopy, implemented on an inverted microscope with a single confocal pinhole shared by the two spectrometers, provides a powerful tool for the combined chemical and mechanical characterisation of contact lenses at the micrometre scale. The automatic matching of the Brillouin and Raman scattering volumes enables simultaneous acquisition of the two signals from the same point.

Applied to Delefilcon A silicone-hydrogel lenses, BRMS has revealed micrometric bulk heterogeneities not previously reported. Their Raman fingerprint identifies them as clusters of the copper phthalocyanine handling tint, whose local aggregation produces the observed optical contrast. Two-dimensional Brillouin mapping shows a reduction of the frequency shift by up to ∼0.5 GHz close to the centre of the clusters. The linewidth–frequency-shift correlation supports a local softening of the longitudinal modulus of up to about 12%, with excess broadening at the cluster boundaries consistent with heterogeneous broadening.

These findings demonstrate that BRMS resolves chemical–mechanical heterogeneities inaccessible to either technique alone, with potential implications for lens durability, and confirm its broader promise for the study of complex soft and biomedical materials.

ACKNOWLEDGEMENTS

We thank Pier Luigi Camiciottoli, Francesco Curci, Andrea Ferrara, Stefano Lorè, and Francesco Ragna for helpful discussions and for providing the analysed samples. This work was funded by the CARIT Foundation Project, call 1/2024 (project code: FCTR24UNIPG) During the preparation of this work the authors used Claude (Anthropic) in order to improve the clarity and readability of the manuscript text. After using this tool, the authors reviewed and edited the content as needed and take full responsibility for the content of the published article.

Open access publishing facilitated by Universita degli Studi di Perugia, as part of the Wiley - CRUI-CARE agreement.

ORCID

Alessandra Anna Passeri https://orcid.org/0009-0009-4614-8960
Martina Alunni Cardinali https://orcid.org/0000-0001-8667-7394
Erika Ponzini https://orcid.org/0000-0002-3103-740X
Daniele Fioretto https://orcid.org/0000-0003-4487-0035

REFERENCES

1. Berne, B. J., & Pecora, R. (2000). *Dynamic light scattering: With Applications to chemistry, biology, and physics*. Dover Publications.
2. Bouvet, P., Bevilacqua, C., Ambekar, Y., Antonacci, G., Au, J., Caponi, S., Chagnon-Lessard, S., Czarske, J., Dehoux, T., Fioretto, D., Fu, Y., Guck, J., Hamann, T., Heinemann, D., Jähnke, T., Jean-Ruel, H., Kabakova, I., Koski, K., Koukourakis, N., … Elsayad, K. (2025). Consensus statement on Brillouin light scattering microscopy of biological materials. *Nature Photonics*, *19*, 681–691.
3. Dil, J. G. (1982). Brillouin scattering in condensed matter. *Reports on Progress in Physics*, *45*, 285.
4. Antonacci, G., Beck, T., Bilenca, A., Czarske, J., Elsayad, K., Guck, J., Kim, K., Krug, B., Palombo, F., Prevedel, R., & Scarcelli, G. (2020). Recent progress and current opinions in Brillouin microscopy for life science applications. *Biophysical Reviews*, *12*, 615–624.
5. Palombo, F., & Fioretto, D. (2019). Brillouin light scattering: Applications in biomedical sciences. *Chemical Reviews*, *119*, 7833–7847.
6. Kabakova, I., Zhang, J., Xiang, Y., Caponi, S., Bilenca, A., Guck, J., & Scarcelli, G. (2024). Brillouin microscopy. *Nature Reviews Methods Primers*, *4*, 8.
7. Scarcelli, G., Besner, S., Pineda, R., Kalout, P., & Yun, S. H. (2015). In vivo biomechanical mapping of normal and keratoconus corneas. *JAMA Ophthalmology*, *133*, 480–482.
8. Randleman, J. B., Zhang, H., Hammoud, B., Dutra, B. A. L., Susanna, B. N., & Scarcelli, G. (2025). Three-dimensional mechanical characterization of normal, subclinical, and keratoconic corneas using motion tracking Brillouin microscopy. *American Journal of Ophthalmology*, *278*, 305–316.
9. Scarponi, F., Mattana, S., Corezzi, S., Caponi, S., Comez, L., Sassi, P., Morresi, A., Paolantoni, M., Urbanelli, L., Emiliani, C., Roscini, L., Corte, L., Cardinali, G., Palombo, F., Sandercock, J. R., & Fioretto, D. (2017). High-performance versatile setup for simultaneous Brillouin-Raman microspectroscopy. *Physical Review X*, *7*, 31015.
10. Ponzini, E., Recchioni, A., Cheloni, R., Zeri, F., & Tavazzi, S. (2023). Physical properties and interaction with the ocular surface of water-gradient contact lenses. *Eye & Contact Lens*, *49*, 152–159.
11. Pruitt, J., Qiu, Y., Thekveli, S., & Hart, R. (2012). Surface characterization of a water gradient silicone hydrogel contact lens (delefilcon A). *Investigative Ophthalmology & Visual Science*, *53*, 6107.

12. Krysztofiak, K., Ciężar, K., & Kościński, M. (2017). Raman imaging of layered soft contact lenses. *Journal of Applied Biomaterials & Functional Materials*, *15*, 149–152.
13. Di Maggio, R., Rossi, F., Fambri, L., & Fontana, A. (2004). Raman and Brillouin scattering measurements on hybrid inorganic–organic materials obtained from tetraethoxysilane and methacrylic monomers. *Journal of Non-Crystalline Solids*, *345–346*, 591–595.
14. Mattana, S., Mattarelli, M., Urbanelli, L., Sagini, K., Emiliani, C., Serra, M. D., Fioretto, D., & Caponi, S. (2018). Non-contact mechanical and chemical analysis of single living cells by microspectroscopic techniques. *Light: Science & Applications*, *7*, 17139.
15. Cardinali, M. A., Passeri, A. A., Bonacci, F., Loré, S., Ponzini, E., Tavazzi, S., & Fioretto, D. (2026). Non-invasive mechano-chemical profiling of delefilcon a contact lenses by Brillouin-Raman microspectroscopy. *Nuovo Cimento della Societa Italiana di Fisica C*. Italian Physical Society.
16. Tavazzi, S., Tonveronachi, M., Fagnola, M., Cozza, F., Ferraro, L., Borghesi, A., Ascagni, M., & Farris, S. (2015). Wear effects on microscopic morphology and hyaluronan uptake in siloxane-hydrogel contact lenses. *Journal of Biomedical Materials Research Part B: Applied Biomaterials*, *103*, 1092–1098.
17. Defeyt, C., Vandenabeele, P., Gilbert, B., Van Pevenage, J., Cloots, R., & Strivay, D. (2012). Contribution to the identification of α-, β- and ε-copper phthalocyanine blue pigments in modern artists' paints by X-ray powder diffraction, attenuated total reflectance micro-fourier transform infrared spectroscopy and micro-Raman spectroscopy. *Journal of Raman Spectroscopy*, *43*, 1772–1780.
18. Basova, T. V., Kiselev, V. G., Schuster, B.-E., Peisert, H., & Chassé, T. (2009). Experimental and theoretical investigation of vibrational spectra of copper phthalocyanine: Polarized single-crystal Raman spectra, isotope effect and DFT calculations. *Journal of Raman Spectroscopy*, *40*, 2080–2087.
19. Londero, P. S., Leona, M., & Lombardi, J. R. (2013). Definitive evidence for linked resonances in surface-enhanced Raman scattering: Excitation profile of Cu phthalocyanine. *Applied Physics Letters*, *102*, 111101.
20. Bailey, M., Alunni-Cardinali, M., Correa, N., Caponi, S., Holsgrove, T., Barr, H., Stone, N., Winlove, C. P., Fioretto, D., & Palombo, F. (2020). Viscoelastic properties of biopolymer hydrogels determined by Brillouin spectroscopy: A probe of tissue micromechanics. *Science Advances*, *6*, eabc1937.
21. Mattarelli, M., Vassalli, M., & Caponi, S. (2020). Relevant length scales in brillouin imaging of biomaterials: The interplay between phonons propagation and light focalization. *ACS Photonics*, *7*, 2319–2328.

How to cite this article: Passeri, A. A., Cardinali, M. A., Ponzini, E., Tavazzi, S., & Fioretto, D. (2026). Brillouin–Raman micro-mapping of silicone-hydrogel contact lenses: Revealing chemical and mechanical heterogeneities. *Journal of Microscopy*, 1–7. https://doi.org/10.1111/jmi.70171